

SIMULTANEOUS OPTIMAL REGULATION OF KINETIC+MAGNETIC SCALAR PLASMA PROPERTIES FOR ROBUST SUSTAINMENT OF ADVANCED SCENARIOS IN NSTX-U

Integrating control objectives by using on-line model-based optimization techniques

H. AL KHAWALDEH, S. T. PARUCHURI, Z. WANG, T. RAFIQ, E. SCHUSTER
 Lehigh University
 Bethlehem, USA
 Email: alkhawaldeh@lehigh.edu

Abstract

A control algorithm based on real time optimization has been developed for the simultaneous regulation of kinetic and magnetic scalar parameters in NSTX-U. This active control algorithm can contribute to operation optimization in tokamaks by regulating advanced scenarios characterized by steady-state operation, stable plasma confinement, and high-performance plasma. Actively shaping plasma profiles such as the safety factor is key in achieving and sustaining these advanced scenarios. However, as the number of control objectives to be addressed simultaneously increases, the profile-control problem may need to be reduced to the regulation of the profile at a few spatial locations due to controllability limits. In this case, the control objectives are reduced to a finite number of scalar plasma parameters, such as plasma-profile values at specific spatial points or volume-averaged plasma properties. On the positive side, effective simultaneous regulation of these scalar parameters may be all what is needed to achieve a desired scenario. A model-based optimal-control algorithm for simultaneous regulation of the central and boundary values of the safety-factor (q) profile, internal inductance (l_i), and normalized beta (β_N) has been developed in this work. The control algorithm has been designed based on control-oriented state models for the poloidal magnetic flux profile (ψ) and the plasma stored energy (W) coupled with output models for q , l_i and β_N . Moreover, in order to demonstrate robustness against model uncertainties, the proposed control algorithm has been tested in higher-fidelity, nonlinear simulations using COTSIM (Control Oriented Transport SIMulator).

1. INTRODUCTION

One of NSTX-U's objectives is to explore the capability of the spherical-tokamak concept to produce and sustain advanced tokamak (AT) scenarios, which are characterized by steady-state operation, stable plasma confinement, and high-performance plasma [1]. The safety factor (q) profile and normalized beta (β_N) are plasma parameters critical to the performance of the confined plasma and its magnetohydrodynamic (MHD) stability. Thus, regulating these parameters simultaneously plays an essential role in achieving AT scenarios. However, varying plasma conditions and external disturbances may make sustaining the desired scenario challenging. Active control could prove useful in regulating these plasma parameters around desired targets in such cases. Therefore, various algorithms have been proposed to tackle this challenging profile-control problem in NSTX-U [2, 3]. However, as the number of control objectives to be addressed simultaneously increases, the profile-control problem may need to be reduced to the regulation of the profile at a few spatial locations due to controllability issues. In such instances, the control goals can be narrowed down to a finite number of scalar plasma properties, such as the values of plasma profiles at specific spatial points or volume-averaged plasma properties. This rationale drives the development of controllers for the simultaneous regulation of scalar plasma parameters. Different feedback control algorithms have been explored for this purpose in different tokamaks such as EAST [4, 5, 6], DIII-D [7, 8], and ITER [9]. Moreover, algorithms for simultaneous control of q and β_N have been proposed for NSTX-U in [10, 11]. This work extends present control capabilities in NSTX-U by increasing the number of simultaneously controlled plasma scalar properties and by providing adaptiveness to changing plasma and device conditions through real-time optimization of the control solution.

A control algorithm based on Model Predictive Control (MPC) (real-time optimization) for simultaneous regulation of the central and boundary values of the safety-factor (q) profile, internal inductance (l_i), and normalized beta (β_N) has been developed in this work. The control algorithm utilizes control-oriented state models for the the poloidal flux gradient (θ) and plasma stored energy (W) coupled with output models for q , l_i and β_N . The controller determines the neutral beam injection (NBI) powers and the overall plasma current that are needed to regulate the desired scalar quantities. The ability to achieve and maintain desired plasma states through feedback algorithms allows for operating at a close proximity to stability limits, exploring plasma regimes of interest, and extracting maximal scientific understanding of the plasma discharges and scenarios under study. The proposed

controller is tested in higher-fidelity nonlinear simulations that employ 1D models for the evolutions of both current and temperature profiles for NSTX-U using the Control Oriented Transport Simulator (COTSIM).

The remainder of this paper is organized as follows. The control-oriented response models are introduced in Section 2. The model reduction, linearization, and discretization, as well as the control-algorithm design are explained in Section 3. Simulations studies assessing the performance of the proposed algorithm are provided in Section 4. Finally, concluding remarks are presented in Section 5.

2. POLOIDAL MAGNETIC FLUX AND ENERGY EVOLUTION MODELS

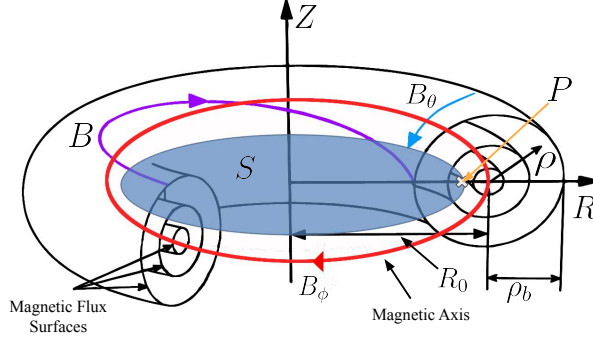


FIG. 1. Magnetic configuration in a tokamak.

The helical magnetic field responsible for confining the plasma within the tokamak is a combination of the toroidal magnetic field denoted as \vec{B}_ϕ and the poloidal magnetic field denoted as \vec{B}_θ . Magnetic field lines encircling the torus map regions with constant poloidal magnetic flux Ψ . At a specific point P , the poloidal magnetic flux is defined as $\Psi \triangleq \int_S \vec{B}_\theta \cdot d\vec{S}$, where \vec{S} represents the surface enclosed by a toroidal ring that crosses P within the poloidal plane, and is perpendicular to the Z axis (as shown in Figure 1). Under ideal MHD conditions, points with constant magnetic flux form nested surfaces [12]. Any parameter that indexes the flux surfaces can serve as a spatial coordinate for describing spatially varying plasma parameters such as the q profile. The chosen spatial coordinate in this work is the mean effective minor radius, which is defined as $\rho \triangleq \sqrt{\Phi / (B_{\phi,0} \pi)}$, where $B_{\phi,0}$ is the vacuum toroidal magnetic field at the magnetic axis, and Φ is the toroidal magnetic flux. The normalized mean effective minor radius is defined as $\hat{\rho} \triangleq \rho / \rho_b$, where ρ_b is the mean effective minor radius of the last closed flux surface.

The q profile is defined as the ratio between the number of times a magnetic field line goes toroidally around the tokamak to the number of times it goes around poloidally,

$$q(\hat{\rho}, t) \triangleq \frac{d\Phi}{d\Psi} = -\frac{B_{\phi,0} \rho_b^2 \hat{\rho}}{\partial \Psi / \partial \hat{\rho}} = -\frac{B_{\phi,0} \rho_b^2 \hat{\rho}}{\theta(\hat{\rho}, t)}, \quad (1)$$

$$\theta(\hat{\rho}, t) \triangleq \frac{\partial \Psi}{\partial \hat{\rho}}, \quad \Psi \triangleq \Psi / (2\pi), \quad (2)$$

where ψ is the poloidal stream function.

2.1. Poloidal Magnetic Flux

The evolution of the poloidal stream function ψ is given by the magnetic diffusion equation (MDE) and its boundary conditions

$$\frac{\partial \psi}{\partial t} = \frac{\eta(T_e)}{\mu \rho_b^2 \hat{F}^2} \frac{1}{\hat{\rho}} \frac{\partial}{\partial \hat{\rho}} \left[\hat{\rho} D_\psi(\hat{\rho}) \frac{\partial \psi}{\partial \hat{\rho}} \right] + R_0 \hat{H} \eta(T_e) \frac{\langle \vec{j}_{ni} \cdot \vec{B} \rangle}{B_{\phi,0}}, \quad (3)$$

$$\frac{\partial \psi}{\partial \hat{\rho}} \Big|_{\hat{\rho}=0} = 0, \quad \frac{\partial \psi}{\partial \hat{\rho}} \Big|_{\hat{\rho}=1} = -\frac{\mu_0 R_0}{2 \hat{G} \hat{H}} I_p, \quad (4)$$

where η is the plasma resistivity, T_e is the electron temperature, μ_0 is the vacuum permeability, R_0 is the major radius, \vec{j}_{ni} is the noninductive current density, \vec{B} is the magnetic field, I_p is the total plasma current, $\langle \cdot \rangle$ denotes a flux-surface average, $D_\psi(\hat{\rho}) \triangleq \hat{F}(\hat{\rho}) \hat{G}(\hat{\rho}) \hat{H}(\hat{\rho})$, \hat{H} , \hat{G} , and \hat{F} are spatially varying geometric factors pertaining to

the magnetic configuration of a particular plasma equilibrium in the form

$$\hat{F} \triangleq \frac{R_0 B_{\phi,0}}{R B_{\phi}(R, Z)}, \quad \hat{G} \triangleq \left\langle \frac{R_0^2}{R^2} |\nabla \rho|^2 \right\rangle, \quad \hat{H} \triangleq \frac{\hat{F}}{\langle R_0^2/R^2 \rangle}. \quad (5)$$

The noninductive current drive is produced by a combination of auxiliary neutral beam drive and the bootstrap current drive, and is expressed as

$$\frac{\langle \bar{j}_{ni} \cdot \bar{B} \rangle}{B_{\phi,0}}(\hat{\rho}, t) = \sum_{i=1}^{n_{nbi}} \frac{\langle \bar{j}_{nbi} \cdot \bar{B} \rangle}{B_{\phi,0}} + \frac{\langle \bar{j}_{bs} \cdot \bar{B} \rangle}{B_{\phi,0}}, \quad (6)$$

where \bar{j}_{nbi} is the noninductive current generated by the NBIs, n_{nbi} is the number of NBIs, and \bar{j}_{bs} is the noninductive current generated by bootstrap effect. In order to use the MDE (3) for control synthesis, control-oriented models for electron temperature, electron density, plasma resistivity, NBI current-drive, and bootstrap current-drive have been used in this work. Detailed description of these models can be found in [11]. Substituting the control oriented models into (3) produces a model of the form

$$\frac{\partial \psi}{\partial t} = f_{\eta}(\hat{\rho}) \frac{\bar{n}_e^{3/2}}{I_p^{3/2} P_{tot}^{3/4}} \frac{1}{\hat{\rho}} \frac{\partial}{\partial \hat{\rho}} \left[\hat{\rho} D_{\psi} \frac{\partial \psi}{\partial \hat{\rho}} \right] + \sum_{i=1}^6 \left[f_i(\hat{\rho}) \frac{P_i}{I_p P_{tot}^{1/2}} \right] + f_{bs}(\hat{\rho}) \frac{\bar{n}_e^{3/2}}{I_p^{1/2} P_{tot}^{1/4}} \left[\frac{\partial \psi}{\partial \hat{\rho}} \right]^{-1}, \quad (7)$$

where f_{η} , f_i , f_{bs} can be expressed in terms of the various model profiles and constants. Differentiating (7) on both sides with respect to the spatial variables $\hat{\rho}$ yields a partial differential equation (PDE) of the form

$$\frac{\partial \theta}{\partial t} = h_0 \frac{\bar{n}_e^{3/2}}{I_p^{3/2} P_{tot}^{3/4}} \theta'' + h_1 \frac{\bar{n}_e^{3/2}}{I_p^{3/2} P_{tot}^{3/4}} \theta' + h_2 \frac{\bar{n}_e^{3/2}}{I_p^{3/2} P_{tot}^{3/4}} \theta + \left[f_{bs} \frac{1}{\theta} \frac{\bar{n}_e^{3/2}}{I_p^{1/2} P_{tot}^{1/4}} \right]' + \sum_{i=1}^6 f_i' \frac{P_i}{I_p P_{tot}^{1/2}}, \quad (8)$$

$$\theta|_{\hat{\rho}=0} = 0, \quad \theta|_{\hat{\rho}=1} = -\frac{\mu_0 R_0}{2 \hat{G} \hat{H}} I_p, \quad (9)$$

where $(\cdot)' = \partial/\partial \hat{\rho}$, h_0 , h_1 , h_2 are expressed in terms of D_{ψ} , f_{η} , and $\hat{\rho}$ [11].

The plasma internal inductance, usually employed as a measure of the θ profile broadness or peakedness, is defined as

$$l_i = \frac{8\pi^2}{\mu_0^2 R_0^2 I_p^2} \int_0^1 \hat{\rho} \hat{G} \hat{H} \frac{\partial \psi}{\partial \hat{\rho}} d\hat{\rho} = \frac{8\pi^2}{\mu_0^2 R_0^2 I_p^2} \int_0^1 \hat{\rho} \hat{G} \hat{H} \theta d\hat{\rho}. \quad (10)$$

2.2. Plasma Stored Energy Dynamics

The evolution of the plasma total energy W can be modeled as

$$\frac{dW(t)}{dt} = -\frac{W(t)}{\tau_E(t)} + P_{tot}(t). \quad (11)$$

The energy confinement time τ_E is calculated using the IPB98(y,2) scaling law and represented as [13]

$$\tau_E = 0.0562 H_H I_p^{0.93} B_T^{0.15} R_0^{0.97} M^{0.19} \varepsilon^{0.58} \bar{n}_{e,19}^{0.41} \kappa^{0.78} P_{tot}^{-0.69}, \quad (12)$$

where H_H is the so-called H-factor, M is the plasma effective mass in amu, $\varepsilon \triangleq a/R_0$ is the inverse aspect ratio, $\bar{n}_{e,19}$ is the line-average electron density in $10^{19} m^{-3}$, and κ is the plasma elongation at the 95% flux surface.

The plasma stored energy W is related to β_N as follows

$$\beta_N = \frac{(2/3)W/V_p a B_{\phi,0}}{B_{\phi,0}^2/(2\mu_0) I_p}, \quad (13)$$

where V_p is the plasma volume, and a is the minor radius of the plasma.

3. MODEL REDUCTION AND CONTROL SYNTHESIS

3.1. Model Reduction Via Spatial Discretization

The model given in (8) is a partial differential equation (PDE). Since a reduced-order model is needed for the synthesis of the feedback controller, (8) is spatially discretized using finite difference approach. The infinite-dimensional model is discretized into n nodes using a uniform grid,

$$\Delta \hat{\rho} = \frac{1}{n-1}, \quad \hat{\rho}_i = (i-1)\Delta \hat{\rho}, \quad i = (1, \dots, n), \quad (14)$$

where θ at $\hat{\rho}_i$ will be denoted as $\theta_i = \theta(\hat{\rho}_i, t)$.

3.2. Model Linearization and Temporal Discretization

The discretized form of the PDE (8) for the poloidal magnetic flux gradient and the ODE (11) for the plasma total energy yield a set of nonlinear ODEs of the form

$$\dot{Z} = f(Z, u), \quad (15)$$

where $Z = [\theta_2, \theta_3, \dots, \theta_{n-1}, W]^T$, $u = [I_p, P_1, P_2, \dots, P_{n_{nb}}]^T$, f is a nonlinear function. Note that the evolution of Z depends on the prescribed term \bar{n}_e . Assuming that the change in \bar{n}_e is insignificant in the flat-top phase makes the above model autonomous. Linearizing (15) is required for the design of the MPC. Thus, a first order Taylor approximation around a reference trajectory is given by

$$\dot{Z} \approx f(Z^{ref}, u^{ref}) + \left. \frac{\partial f}{\partial Z} \right|_{Z^{ref}, u^{ref}} (Z - Z^{ref}) + \left. \frac{\partial f}{\partial u} \right|_{Z^{ref}, u^{ref}} (u - u^{ref}), \quad (16)$$

where the reference trajectory state Z^{ref} and input u^{ref} satisfies

$$\dot{Z}^{ref} = f(Z^{ref}, u^{ref}). \quad (17)$$

By defining $\bar{Z} = Z - Z^{ref}$, and $\bar{u} = u - u^{ref}$, (16) becomes

$$\dot{\bar{Z}} = A\bar{Z} + B\bar{u}, \quad (18)$$

$$A \triangleq \left. \frac{\partial f}{\partial Z} \right|_{Z^{ref}, u^{ref}}, \quad B \triangleq \left. \frac{\partial f}{\partial u} \right|_{Z^{ref}, u^{ref}}. \quad (19)$$

As the control objective is to track a desired output trajectory, namely the q , β_N , and l_i , the state equation (18) needs to be complemented with an output equation. If the output equations of q , β_N , and l_i take the form,

$$y = f_y(Z, u), \quad y \triangleq [q, \beta_N, l_i]^T, \quad (20)$$

and by defining $\bar{y} = y - y^{ref} = [\bar{q}, \bar{\beta}_N, \bar{l}_i]^T$, then a similar approach to (15)-(19) can be applied to yield

$$\dot{\bar{y}} = C\bar{Z} + D\bar{u}, \quad (21)$$

$$C \triangleq \left. \frac{\partial f_y}{\partial Z} \right|_{Z^{ref}, u^{ref}}, \quad D \triangleq \left. \frac{\partial f_y}{\partial u} \right|_{Z^{ref}, u^{ref}}. \quad (22)$$

The model described in (18) and (21) represents a continuous-time linear system. Model predictive control algorithms require discrete-time models to facilitate their practical implementation in the plasma control system. Therefore, it is essential to perform a temporal discretization of (18) and (21) using zero-order hold discretization with sampling period T . If the time step $t_k = kT$, then the discrete-time system dynamics is presented as

$$\bar{Z}(t_{k+1}) = A_d \bar{Z}(t_k) + B_d \bar{u}(t_k), \quad (23)$$

$$\bar{y}(t_k) = C_d \bar{Z}(t_k) + D_d \bar{u}(t_k), \quad (24)$$

where $A_d = (I_{n-1 \times n-1} - AT)^{-1}$, $B_d = (I_{n-1 \times n-1} - AT)^{-1}BT$, $C_d = C$, $D_d = D$.

3.3. Control Synthesis

The primary aim of this work is to develop, and assess feedback control algorithm for q , l_i , and β_N . The control oriented models discussed in previous sections have been effectively integrated into an MPC framework to construct a controller with the ability to govern the scalar properties $q(\hat{p} = 0.05, 0.95)$, l_i , β_N . Model Predictive Control (MPC) is a control strategy that optimizes future control actions by repeatedly solving an online optimization problem based on a predictive model of the system while accounting for constraints. The general procedure for implementing MPC in the plasma control system can be summarized as follows:

- (i) At time step t_k , the state sample $x(t_k)$ is transferred to the controller.
- (ii) The controller solves an N -step optimal control problem subject to state evolution and input constraints. The result of optimization is a vector of optimal inputs each corresponding to the time-steps in the finite horizon.

(iii) The input value corresponding to the first time step of the optimal input vector is implemented in the system.

(iv) At the next time step t_{k+1} , the above process is repeated again.

Standard MPC algorithms, while highly effective for controlling dynamic systems, do not achieve integral action. However, an integral action is required to eliminate any steady state error. A method for incorporating an integrator within the MPC framework is to modify the plant so that the input is the control increment $\Delta\bar{u}(t_k) = \bar{u}(t_k) - \bar{u}(t_{k-1})$, rather than $\bar{u}(t_k)$ [14]. Such a model can be derived from (23), (24) and takes the form

$$\Delta\bar{Z}(t_{k+1}) = A_d\Delta\bar{Z}(t_k) + B_d\Delta\bar{u}(t_k), \quad (25)$$

$$\Delta\bar{y}(t_k) = C_d\Delta\bar{Z}(t_k) + D_d\Delta\bar{u}(t_k), \quad (26)$$

where $\Delta\bar{Z}(t_k) = \bar{Z}(t_k) - \bar{Z}(t_{k-1})$, and $\Delta\bar{y}(t_k) = \bar{y}(t_k) - \bar{y}(t_{k-1})$. Finally, defining a new state vector as $x(t_k) = [\Delta\bar{Z}(t_k) \quad \bar{y}(t_{k-1})]^T$, (25) and (26) can be combined to form the augmented model

$$x(t_{k+1}) = \bar{A}x(t_k) + \bar{B}\Delta\bar{u}(t_k), \quad (27)$$

$$\bar{y}(t_k) = \bar{C}x(t_k) + \bar{D}\Delta\bar{u}(t_k), \quad (28)$$

$$\bar{A} = \begin{bmatrix} A_d & 0 \\ C_d & I_{n_y \times n_y} \end{bmatrix}, \quad \bar{B} = \begin{bmatrix} B_d \\ D_d \end{bmatrix}, \quad \bar{C} = \begin{bmatrix} C_d^T \\ I_{n_y \times n_y} \end{bmatrix}^T, \quad \bar{D} = D_d, \quad (29)$$

where n_y is the number of outputs. The new augmented system shown in (27)-(28) can be used to define a Prediction Model (PM) for a finite horizon N [15]

$$\bar{y}_{k|N} = O_N x(t_k) + F_N \Delta\bar{u}_{k|N}, \quad (30)$$

$$\bar{y}_{k|N} = [\bar{y}(t_k)^T \quad \bar{y}(t_{k+1})^T \quad \bar{y}(t_{k+2})^T \quad \dots \quad \bar{y}(t_{k+N})^T]^T, \quad (31)$$

$$\Delta\bar{u}_{k|N} = [\Delta\bar{u}(t_k)^T \quad \Delta\bar{u}(t_{k+1})^T \quad \Delta\bar{u}(t_{k+2})^T \quad \dots \quad \Delta\bar{u}(t_{k+N})^T]^T, \quad (32)$$

$$O_N = [(\bar{C})^T \quad (\bar{C}\bar{A})^T \quad (\bar{C}\bar{A}^2)^T \quad \dots \quad (\bar{C}\bar{A}^{N-1})^T]^T, \quad (33)$$

$$F_N = \begin{bmatrix} \bar{D} & 0 & 0 & 0 & \dots & 0 \\ \bar{C}\bar{B} & \bar{D} & 0 & 0 & \dots & 0 \\ \bar{C}\bar{A}\bar{B} & \bar{C}\bar{B} & \bar{D} & 0 & \dots & 0 \\ \bar{C}\bar{A}^2\bar{B} & \bar{C}\bar{A}\bar{B} & \bar{C}\bar{B} & \bar{D} & \dots & 0 \\ \vdots & \vdots & \vdots & \ddots & \ddots & 0 \\ \bar{C}\bar{A}^{N-1}\bar{B} & \bar{C}\bar{A}^{N-2}\bar{B} & \dots & \bar{C}\bar{A}\bar{B} & \bar{C}\bar{B} & \bar{D} \end{bmatrix}. \quad (34)$$

3.4. Control Input Constraints

Let $\bar{u}_{max} = u_{max} - u^{ref}$ and $\bar{u}_{min} = u_{min} - u^{ref}$ define the input limits for the actuators. Hence, it is possible to write

$$\bar{u}_{min|N} \leq \bar{u}_{k|N} \leq \bar{u}_{max|N}, \quad (35)$$

$$\bar{u}_{k|N} = [\bar{u}(t_k)^T \quad \bar{u}(t_{k+1})^T \quad \bar{u}(t_{k+2})^T \quad \dots \quad \bar{u}(t_{k+N})^T]^T, \quad (36)$$

$$\bar{u}_{max|N} = [\bar{u}_{max}^T \quad \bar{u}_{max}^T \quad \bar{u}_{max}^T \quad \dots \quad \bar{u}_{max}^T]^T, \quad (37)$$

$$\bar{u}_{min|N} = [\bar{u}_{min}^T \quad \bar{u}_{min}^T \quad \bar{u}_{min}^T \quad \dots \quad \bar{u}_{min}^T]^T. \quad (38)$$

Using the definition of $\Delta\bar{u}(t_k)$ recursively, it is possible to obtain the following

$$\bar{u}_{k|N} = S\Delta\bar{u}_{k|N} + c\bar{u}(t_{k-1}), \quad (39)$$

where S is a lower triangular matrix with an identity matrix I_m for its non-zero elements, $c = [I_m \quad I_m \quad \dots \quad I_m]^T$, and m is the number of control inputs. Substituting (39) into (35), the inequality for the future feedback control increment becomes

$$\bar{u}_{min|N} - c\bar{u}(t_{k-1}) \leq S\Delta\bar{u}_{k|N} \leq \bar{u}_{max|N} - c\bar{u}(t_{k-1}). \quad (40)$$

The constraints presented in (40) are equivalent to

$$S\Delta\bar{u}_{k|N} \leq \bar{u}_{max|N} - c\bar{u}(t_{k-1}), \quad (41)$$

$$-S\Delta\bar{u}_{k|N} \leq -\bar{u}_{min|N} + c\bar{u}(t_{k-1}), \quad (42)$$

which can be compactly written as $\alpha\Delta\bar{u}_{k|N} \leq \beta$ with

$$\alpha = \begin{bmatrix} S \\ -S \end{bmatrix}, \quad \beta = \begin{bmatrix} \bar{u}_{max|N} - c\bar{u}(t_{k-1}) \\ -\bar{u}_{min|N} + c\bar{u}(t_{k-1}) \end{bmatrix}. \quad (43)$$

3.5. Quadratic programming

The objective is to track the target scalars with minimum control effort. Thus, the cost function takes the form

$$J(t_k) = [\bar{y}_{k|N} - \bar{y}_{k|N}^d]^T Q [\bar{y}_{k|N} - \bar{y}_{k|N}^d] + \Delta \bar{u}_{k|N}^T R \Delta \bar{u}_{k|N}, \quad (44)$$

where $\bar{y}_{k|N}^d = [\bar{y}_d(t_k) \ \bar{y}_d(t_{k+1}) \ \bar{y}_d(t_{k+2}) \ \dots \ \bar{y}_d(t_{k+N})]$, $\bar{y}_d = y^{tar} - y^{ref}$ is the difference between the target and the reference outputs, y^{tar} is the target output, and Q, R are diagonal weight matrices. Combining the cost function (44) with the PM (30) and the inequality constraint (43), the model predictive control problem can be formulated as

$$\Delta \bar{u}_{k|N}^* = \underset{\Delta \bar{u}_{k|N}}{\text{arg min}} (\Delta \bar{u}_{k|N}^T H \Delta \bar{u}_{k|N} + 2f^T \Delta \bar{u}_{k|N}), \quad (45)$$

$$\text{such that } \alpha \Delta \bar{u}_{k|N} \leq \beta, \quad (46)$$

where $H = F_N^T Q F_N + R$, and $f = (F_N^T Q O_N)x(t_k) - (F_N^T Q)\bar{y}_{k|N}^d$. This defines a standard Quadratic Programming (QP) problem in terms of the unknown future feedback control increments, $\Delta \bar{u}_{k|N}$. A receding horizon strategy is used and only the first control increment $\Delta \bar{u}^*(t_k)$ in the calculated $\Delta \bar{u}_{k|N}^*$ is used for computing the feedback control action $\bar{u}(t_k)$, that can be expressed as

$$\bar{u}(t_k) = \Delta \bar{u}^*(t_k) + \bar{u}(t_{k-1}). \quad (47)$$

4. ASSESSMENT OF CONTROL PERFORMANCE IN SIMULATION STUDIES

The control algorithm developed within this work exploits NSTX-U's capability of driving non-inductive current and heating to the plasma through the recently upgraded NBI system. Therefore, in addition to determining the plasma current, the proposed algorithm determines the NBI powers in order to regulate the desired scalar properties $q(\hat{\rho} = 0.05)$, $q(\hat{\rho} = 0.95)$, l_i , and β_N . In this simulation study, the MPC controller introduced in Section 3 has been tested using COTSIM. This one-dimensional control-oriented transport code plays an important role in assessing the performance of the controller. In this study, the code has combined the MDE with the Electron Heat Transport Equation (EHTE). COTSIM offers a range of analytical models, including neoclassical transport models like Chang-Hinton, electron heat transport via the paleoclassical model, and anomalous transport models such as Bohm/gyro-Bohm and Coppi-Tang. The Chan-Hinton and Bohm/gyro-Bohm models have been used in this study. Furthermore, the current, torque, and heating depositions by the neutral beam injectors have been modeled using a neural-network surrogate model, NUBEAMNet [16], which reproduces the results of NUBEAM in a fraction of the computation time demanded by the original Monte Carlo code. To generate the target for the simulation study, a simulation has been conducted first in COTSIM with arbitrary inputs. This process guarantees feasible targets for $q(\hat{\rho} = 0.05)$, $q(\hat{\rho} = 0.95)$, l_i , and β_N . The plasma current, 2nd, and 4th NBIs have been chosen as available for actuation. Two feedback (FB) simulation cases are presented below to illustrate the performance of the proposed MPC. The two cases differ in the choice of variables controlled by the MPC algorithm. For case 1, the controller tracks ($q(\hat{\rho} = 0.95)$), (β_N), and (l_i); whereas for case 2, the controller tracks ($q(\hat{\rho} = 0.95)$), ($q(\hat{\rho} = 0.05)$), and (β_N). Both cases use the same feedforward (FF) input, which has been selected as constant (constant after the ramp-up phase in the case of the plasma current). The results in Fig. 2 and Fig. 3 compare FF-only (dashed-dotted magenta lines), FF+FB (solid blue lines), and target (dashed red lines) evolutions.

4.1. Case 1

Fig. 2 shows the time evolutions of $q(\hat{\rho} = 0.95)$, β_N , l_i , and the corresponding actuator trajectories I_p , P_{NBI2} , and P_{NBI4} . From the onset of the simulations, it is clear that the FF-only and target trajectories exhibit noticeable disparities. However, the feedback-control scheme is activated at around $t = 2$ seconds. This intervention triggers an immediate correction in response to the deviation between actual and target trajectories. This correction mechanism involves adjusting the actuator inputs to enable efficient tracking of the target trajectory.

4.2. Case 2

Fig. 3 shows the time evolutions of $q(\hat{\rho} = 0.95)$, $q(\hat{\rho} = 0.05)$, (β_N), and the same set of actuators. In this particular case, the target scenario remains identical to that of the first case but it is characterized by a different set of plasma properties. As it was illustrated for the previous case, the control scheme succeeds once again in correcting the FF-only actuation in order to track the desired targets. The FF+FB evolutions converges to the targets within a short time interval after the controller's activation at $t = 2$ seconds. Regardless of the difference in the control objective, the controller is capable of recovering the control inputs that are consistent with the desired scenario.

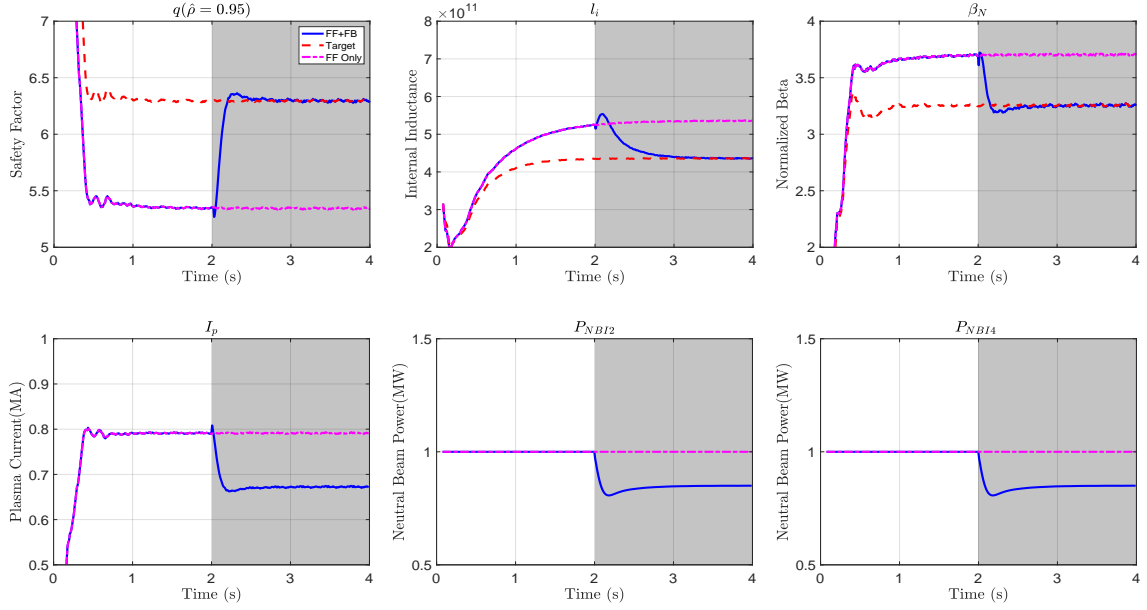


FIG. 2. Time evolution of feedforward-only(Dashed Magenta), feedforward + feedback(Solid Blue), and target plasma properties(Dashed Red). Each of the plots demonstrates the time evolution of the boundary safety factor ($q(\hat{\rho} = 0.95)$), normalized beta (β_N), internal inductance (l_i), plasma current I_p , second NBI power P_{NBI2} , and fourth NBI power P_{NBI4} .

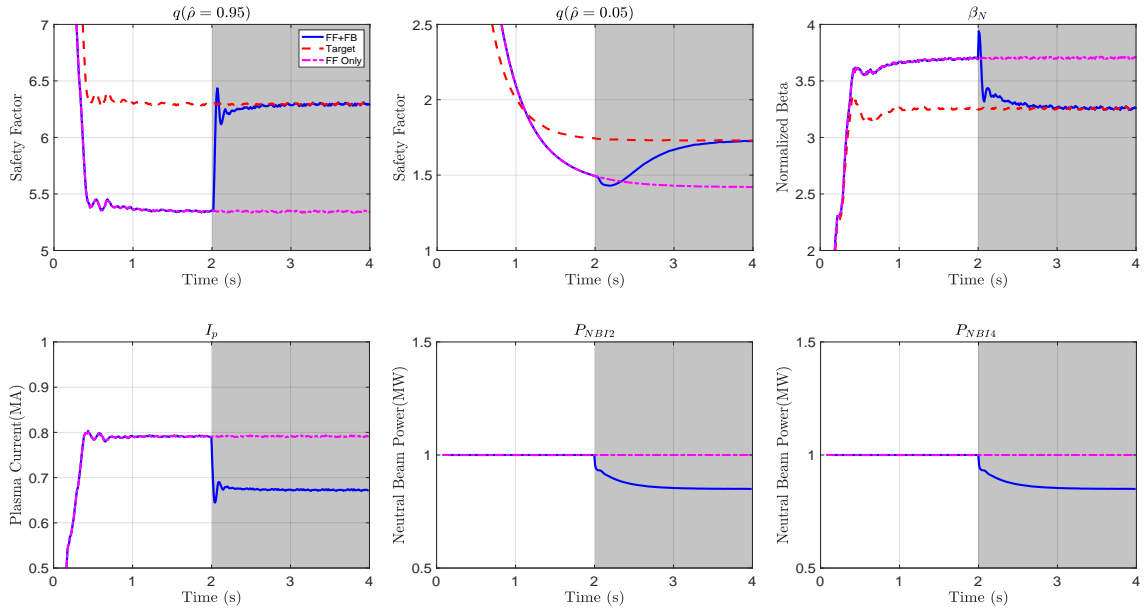


FIG. 3. Time evolution of feedforward-only(Dashed Magenta), feedforward + feedback(Solid Blue), and target plasma properties(Dashed Red). Each of the plots demonstrates the time evolution of the boundary safety factor ($q(\hat{\rho} = 0.95)$), central safety factor ($q(\hat{\rho} = 0.05)$), normalized beta (β_N), plasma current I_p , second NBI power P_{NBI2} , and fourth NBI power P_{NBI4} .

5. CONCLUSION

A control algorithm has been designed based on real-time optimization for the simultaneous regulation of kinetic and magnetic scalar plasma properties in NSTX-U. Linearized control-oriented models that govern the evolutions

of both θ and W have been developed and augmented with output equations for q , β_N , and l_i with the ultimate goal of synthesizing an MPC controller. The proposed controller extends present capabilities at NSTX-U by advancing control integration and increasing adaptiveness through real-time optimization. COTSIM-based higher-fidelity nonlinear simulations show that the controller is capable of efficiently tracking the desired $q(\hat{\rho} = 0.05)$, $q(\hat{\rho} = 0.95)$, l_i , and β_N in NSTX-U. By means of these simulations, the proposed controller has shown robust tracking capabilities even in the presence of model uncertainties and unknown dynamics arising from the differences between synthesis and simulation models. The nonlinear models used in the simulation study offers a significantly higher level of complexity in comparison to the control-oriented models (Section 2) used to synthesize the controller. While, these control solutions are being developed for NSTX-U, they can be extended to support efforts towards realization and robust sustainment of advanced scenarios in any tokamak device.

ACKNOWLEDGMENTS

This material is based upon work partly supported by the U.S. Department of Energy, Office of Science, Office of Fusion Energy Sciences, under Award DE-SC0021385.

DISCLAIMER

This report was prepared as an account of work sponsored by an agency of the US Government. Neither the US Government nor any agency thereof, nor any of their employees, makes any warranty, express or implied, or assumes any legal liability or responsibility for the accuracy, completeness, or usefulness of any information, apparatus, product, or process disclosed, or represents that its use would not infringe privately owned rights. Reference herein to any specific commercial product, process, or service by trade name, trademark, manufacturer, or otherwise, does not necessarily constitute or imply its endorsement, recommendation, or favoring by the US Government or any agency thereof. The views and opinions of authors expressed herein do not necessarily state or reflect those of the US Government or any agency thereof.

DISCLAIMER

This report was prepared as an account of work sponsored by an agency of the US Government. Neither the US Government nor any agency thereof, nor any of their employees, makes any warranty, express or implied, or assumes any legal liability or responsibility for the accuracy, completeness, or usefulness of any information, apparatus, product, or process disclosed, or represents that its use would not infringe privately owned rights. Reference herein to any specific commercial product, process, or service by trade name, trademark, manufacturer, or otherwise, does not necessarily constitute or imply its endorsement, recommendation, or favoring by the US Government or any agency thereof. The views and opinions of authors expressed herein do not necessarily state or reflect those of the US Government or any agency thereof.

REFERENCES

- [1] GERHARDT, S., ANDRE, R., and MENARD, J., Nuclear Fusion **52** (2012) 083020.
- [2] ILHAN, Z. O., BOYER, M. D., and SCHUSTER, E., Fusion Engineering and Design **146** (2019) 555, SI:SOFT-30.
- [3] ILHAN, Z. O., WEHNER, W. P., and SCHUSTER, E., Model predictive control with integral action for the rotational transform profile tracking in NSTX-U, in *2016 IEEE Conference on Control Applications (CCA)*, pp. 623–628, 2016.
- [4] WANG, S., WITRANT, E., and MOREAU, D., Fusion Engineering and Design **162** (2021) 112071.
- [5] WANG, Z., WANG, H., SCHUSTER, E., et al., Optimal shaping of the safety factor profile in the EAST tokamak, in *2021 IEEE Conference on Control Technology and Applications (CCTA)*, pp. 63–68, 2021.
- [6] WANG, H., WEHNER, W. P., and SCHUSTER, E., Combined current profile and plasma energy control via model predictive control in the EAST tokamak, in *2018 26th Mediterranean Conference on Control and Automation (MED)*, pp. 1–9, 2018.
- [7] PAJARES, A. and SCHUSTER, E., Nuclear Fusion **61** (2021) 036006.
- [8] SHI, W., WEHNER, W., BARTON, J., et al., PTRANSP simulation and experimental test of a robust current profile and β_n controller for off-axis current drive scenarios in the DIII-D tokamak, in *2013 American Control Conference*, pp. 1225–1230, 2013.
- [9] BARTON, J. E., BESSEGHIR, K., LISTER, J., and SCHUSTER, E., Plasma Physics and Controlled Fusion **57** (2015) 115003.
- [10] BOYER, M., ANDRE, R., GATES, D., et al., Nuclear Fusion **55** (2015) 053033.
- [11] ALKHAWALDEH, H., LEARD, B., PARUCHURI, S. T., RAFIQ, T., and SCHUSTER, E., Fusion Engineering and Design **192** (2023) 113795.
- [12] WESSON, J. and CAMPBELL, D. J., *Tokamaks*, Oxford University Press, 2018.
- [13] ITER Physics Expert Group on Confinement and Transport and ITER Physics Expert Group on Confinement Modelling and Database and ITER Physics Basis Editors, Nuclear Fusion **39** (1999) 2175.
- [14] CAMACHO, E. F. and BORDONS, C., *Model predictive control by Eduardo F. Camacho and Carlos Bordons*, Springer-Verlag Ltd, 2007.
- [15] RUSCIO, D., Modeling, Identification and Control: A Norwegian Research Bulletin **34** (2013) 119.
- [16] BOYER, M., KAYE, S., and ERICKSON, K., Nuclear Fusion **59** (2019) 056008.